A Facility for Measuring Quantum Cavity Modulated Lepton-Catalyzed Nuclear Fusion

Rhett Lundell

A senior thesis submitted to the faculty of
Brigham Young University
in partial fulfillment of the requirements for the degree of

Bachelor of Science

John Ellsworth and David Allred, Advisors

Department of Physics and Astronomy

Brigham Young University

ABSTRACT

A Facility for Measuring Quantum Cavity Modulated Lepton-Catalyzed Nuclear Fusion

Rhett Lundell
Department of Physics and Astronomy, BYU
Bachelor of Science

Quantum Vacuum Field (QVF) cavities are thought to be able to influence fusion rates of deuterium nuclei. Lepton-catalyzed fusion has been explored extensively for muons. Electrons, another lepton, are proposed to also catalyze fusion under the proper conditions. This paper explores the creation of a facility for measuring an increase in spontaneous fusion rates of deuterons from QVF cavities. I constructed a vacuum system to conduct QVF experiments as well as a physical vapor deposition chamber for cavity preparation. I determined that the facility is not yet able to take data and test the theory, but it can be fully prepared with more work. Further work is also required to conduct the experiment to test the theory of QVF modulated lepton-catalyzed nuclear fusion.

Keywords: Fusion, Electron Screening, Cavity, Neutron Detection, Zero-Point Energy, Lepton-Catalyzed Fusion, Physical Vapor Deposition

ACKNOWLEDGMENTS

I would like to acknowledge my advisors, John Ellsworth and David Allred, for their support and guidance in helping me conduct research and write my thesis, and Dr. Allred specifically for funding support. I would also like to acknowledge my wife, Becca, for always being there for me. I am also grateful to the College of Computational, Mathematical, and Physical Sciences and the Department of Physics and Astronomy for providing the facilities necessary to conduct this research. Finally, I would like to acknowledge my lab mates, Tyler Hamm and Isaac Willden.

Contents

List of Figures

Chapter 1

Introduction

1.1 History of Lepton-Catalyzed Fusion

The Sun gives off energy through the process of nuclear fusion. It is the prime example for fusion energy. However, most current efforts to achieve fusion in the laboratory use particles that are several orders of magnitude more energetic than the Sun. Tokamak reactors use plasmas at billions of degrees, or several MeV, while the Sun operates at a couple million degrees, or about 1 keV. This is because while reactors try to achieve fusion by making particles energetic enough to overcome the Coulomb potential barrier, the Sun fuses hydrogen nuclei through quantum tunneling. The rate at which two protons fuse to form deuterium in the Sun is only on the order of $10^{-18}s^{-1}$ per proton [1].

A decrease in the Coulomb barrier will increase the tunneling rate. The Sun achieves this through stellar plasma screening effects, which aid the sheer mass and quantity of particles in catalyzing fusion. The positive ions in the plasma polarize the surrounding electrons and ions [2]. This screening effectively shields the charge of the nucleus from other nuclei. Another way to shield the nucleus is to replace the electron in a hydrogen atom with a muon. The theory of muon catalyzed fusion was proposed by Frank in 1947 [3] and possibly by Sakharov in 1948 [4]. Frank analyzed data from nuclear reactions on radiological photographic film and argued that a nucleus could be shielded by a negatively charged muon lepton, which would replace the electron in a hydrogen isotope. Since the muon is heavier than the electron, quantum mechanics predicts that it would spend more time closer to the nucleus than an electron. The muonic atom has a reduced charge radius, with the Bohr radius decreasing by a factor of 207 since the muon is 207 times heavier than the electron. In the presence of a second hydrogen isotope, the Gamow barrier would be low as the muonic atom appears neutral until the separation is within the charge radius. The reduced barrier leads to increased tunneling, and the separation of the two nuclei would be within the reach of the strong force, leading to fusion. Without a muon, the reaction $p + D \rightarrow He^3 + \gamma$ releases energy in the form of a gamma ray, as seen. In the case of muon-catalyzed fusion, the reaction would preferentially release energy in the form of momentum transfer to the muon instead of the slower electromagnetic process of creating a gamma ray. The muon would thus be ejected from the atom instead of a gamma ray, with energy similar to that of the gamma. Frank proposed the following equation:

$$H_1^1 D_1^2 (Y^-) \; \rightarrow \; He_2^3 \; + \; Y^- \; + \; 5.46 \, MeV \tag{1.1}$$

This reaction was experimentally observed by Alvarez in 1957 [5]. Alvarez reported seeing a muon catalyze fusion by tracking it in a hydrogen bubble chamber. The curvature of the tracks in the bubble chamber were analyzed to determine the particle type and energy. The tracks showed a muon being captured and then ejected with the energy of Frank's proposed reaction equation, supporting Frank's hypothesis.

Steven Jones in 1986 was the first to suggest that another lepton, an electron, could catalyze this reaction [6]. One of his many experiments, published in 2004, dealt with deuterating titanium foils and measuring their charged particle emissions in a vacuum [7]. John Ellsworth proposed scratching the foils with a razor blade and observed that when the foils were intentionally scratched, the reproducibility of the experiment increased [8]. Other groups have seen electrons ejected from p-d fusion reactions with the reaction energy, 5.6 MeV, supporting Jones' theory of electron-catalyzed fusion. [9].

1.2 Motivation for Using Cavities

To know if an experiment shows an increase in fusion rates, a baseline is needed for reference. Deuterium sitting in a bottle at room temperature is estimated to fuse at a rate of 10^{-64} s^{-1} [10]. Jones observed rates of up to 10^{-21} s^{-1} in his deuterated metal foil experiment [7]. This much closer to the order of magnitude of fusion rates in the Sun. John Ellsworth theorized that the increased fusion rates could be a result of cavities on the surface of the foil moderating the Quantum Vacuum Field (QVF), which led him to propose scratching the foils. The scratching introduced defects onto the surface of the metal, which were proposed to have acted as QVF cavities. One example of cavities moderating the QVF is uncharged conducting parallel plates in a vacuum attract. In 1948 Casimir showed that effect is a result of the zero-point field, another name for the QVF [11]. This cavity induced moderation may affect the deuterium atom. Puthoff found in 1987 that the ground state of hydrogen can be modeled as a QVF determined state [12]. This means that a change in the QVF should influence the charge radius of the electron, potentially allowing it to shrink closer to the nucleus.

This thesis shows the development and testing of a facility for measuring QVF cavity modulated lepton-catalyzed D-D fusion. It discusses the experimental setup, including the detectors used and procedures for creating the cavity. The resulting data shows that the facility is not yet fully equipped for measuring the cavity's effect. With more preparation, the facility will be able to test the theory. If the desired effect is seen after experiment, it will support the proposition that QVF cavities can increase rates of lepton-catalyzed D-D fusion.

Chapter 2

Methods

This chapter discusses the process for making the QFV cavity, creating a vacuum system for the experiment, and the detectors. To make the cavity, I built a Physical Vapor Deposition (PVD) chamber.

2.1 Creating the Cavity

To make the cavity, the goal is to use a silicon wafer and a charged particle detector separated by nanometers. The detector is a surface barrier detector (SBD) for charged particles. The working principle of the SBD is explained in Sec. 2.3. The detector face is flat and made of silicon coated with a layer of aluminum. By pushing a silicon wafer up against the detector face, a cavity is easily formed between parallel plates. The detector, being half of the cavity, allows a convenient way to measure any fusion reaction products.

I wanted a precise way to fix the separation distance between the SBD and the silicon wafer to control the size of the cavity. To get this precise cavity separation, I constructed a PVD chamber system equipped for both sputtering and thermal deposition. The inside of the PVD chamber can be seen in Fig. 2.1. I designed and fabricated a long target holder and shutter system to hold the target

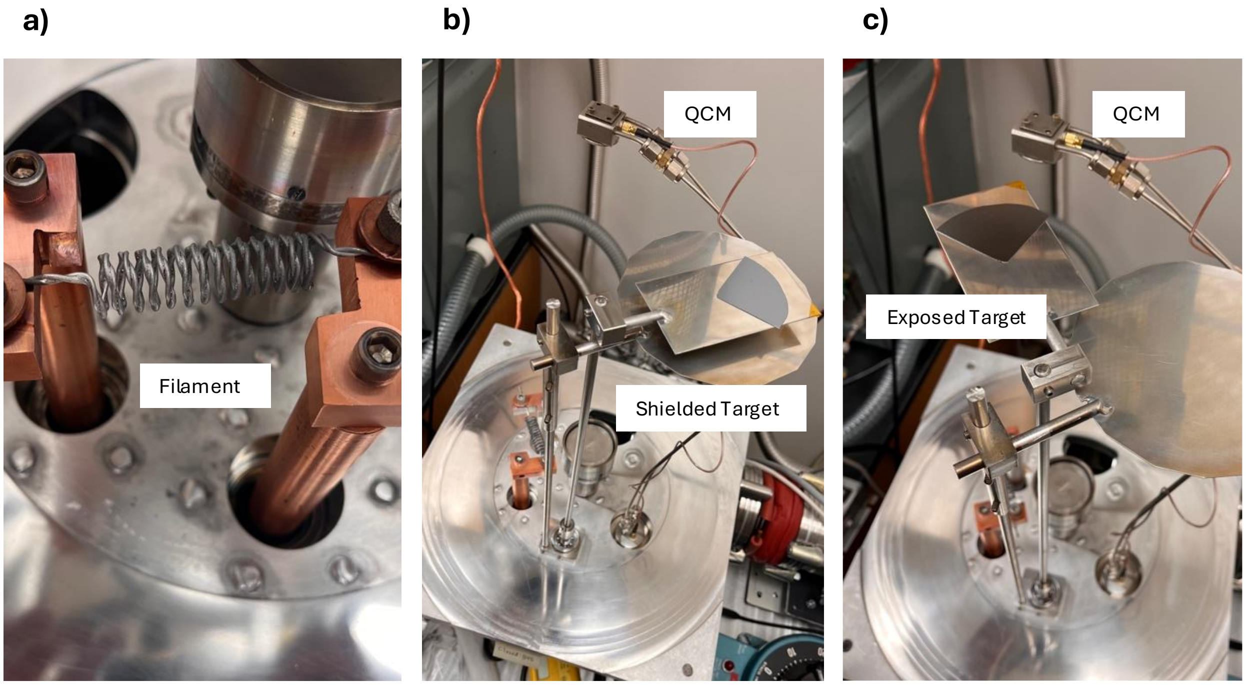

Figure 2.1 Inside of the PVD chamber. a) The filament used to heat the aluminum substrate for deposition. b) The target in shielded position. c) The target holder exposed. The Quartz Crystal Monitor (QCM) can also be seen. The target is held 12 inches above the deposition sources. The QCM is coplanar with the target for better calibration.

significantly far from the source so that deposition would be uniform. A Quartz Crystal Monitor (QCM) ensured that the thickness of material deposited onto the target could be determined. The QCM is calibrated using ellipsometry modeling. The initial design of the shutter blocked the source as it heated up because the substrate evaporates isotropically when it is at a constant temperature, but unevenly as it heats up. The later design blocked only the target, leaving the QCM exposed to the source constantly.

Three legs of aluminum were deposited on the wafer in a tripod shape (see Fig. 2.2). Since the detector is coated with a layer of aluminum, the same material was used for the tripod. A shadow mask ensured all three legs could be deposited at the same time to have the same thickness. The thickness was confirmed using ellipsometry techniques.

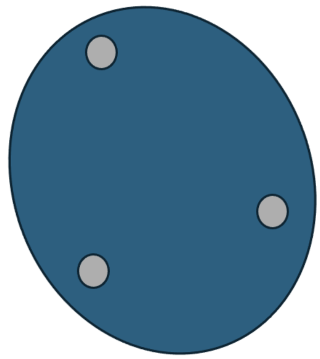

Figure 2.2 3 legs of aluminum deposited on a silicon wafer using a shadow mask to ensure equal thickness.

Fusion reactions need a fuel. A monolayer of deuterium, an isotope of hydrogen, on the wafer would supply the needed fuel for fusion. Atomic hydrogen isotopes are more likely to create a monolayer than molecular hydrogen isotopes as they are more reactive [13]. Surface adsorption of gasses is a natural phenomenon in vacuum systems. Atomic deuterium adsorbs more readily onto surfaces compared with the molecular form, creating a monolayer from the adsorption. I equipped the vacuum system with an RF plasma generator from a plasma cleaning device to ionize deuterium gas and separate the molecules into atomic deuterium. A test in air ensured the plasma generator worked with the system. Plasma created from air can be seen in Fig. 2.3. However, isotopes of hydrogen gas are also dangerous to work with. Hydrogen can potentially explode, so strict standard operating procedures need to be followed. The scope of this thesis does not cover tests with hydrogen in the chamber.

To push the wafer up against the target, I used a plunger adapter on the vacuum system. A spring between the wafer and plunger limited the force on the detector, which is fragile and expensive. If the plunger is pushed too far, it will put pressure on the detector face and shatter it. A model of

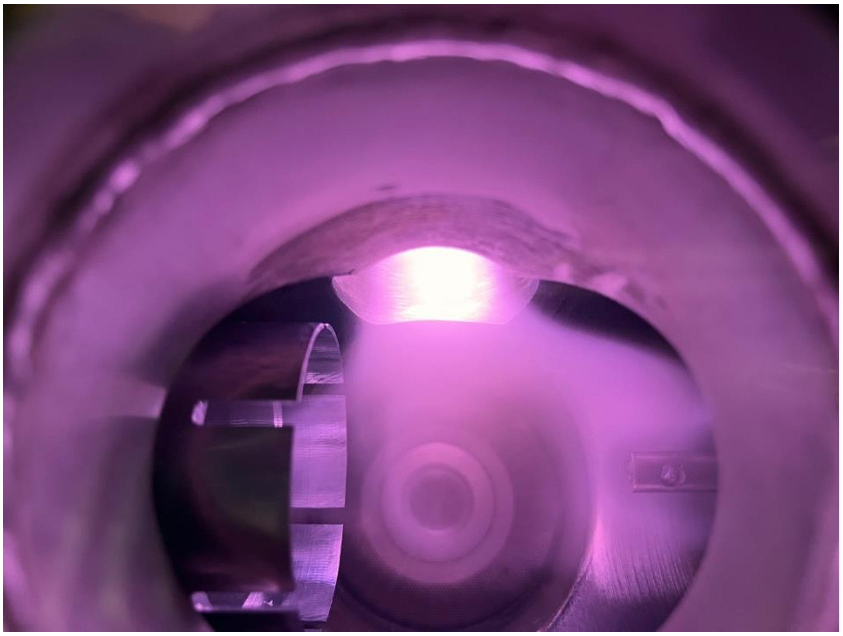

Figure 2.3 Air plasma in the vacuum chamber from the RF plasma generator. The air plasma is able to clean the chamber, which must be done before experiment. The generator is also necessary to ionize deuterium gas for the experiment.

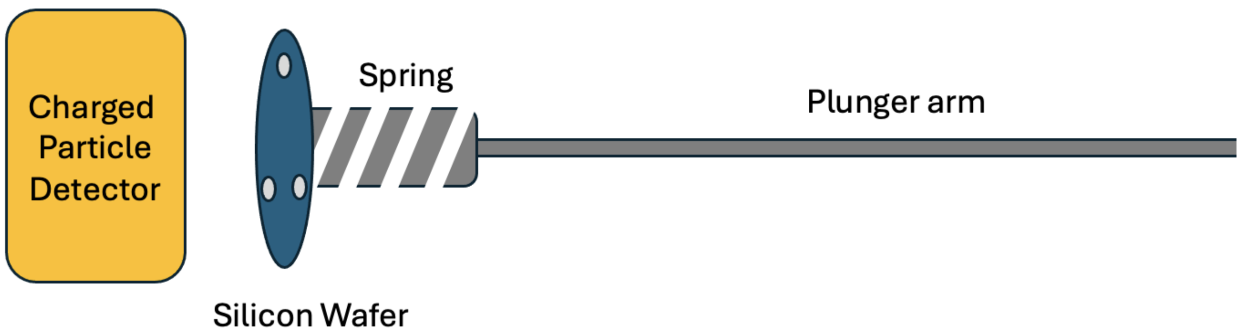

Figure 2.4 The silicon wafer can be moved up against the charged particle detector without risking it breaking because of the spring that relieves force.

what the detector looks like in the vacuum system is given in Fig. 2.4, and the actual picture of the detector is shown in Fig. 2.5. A holder for a vernier micrometer head was designed to precisely control where the wafer would stop when the plunger was fully pushed in. This eliminated the possibility of inserting the plunger too far and also stopped the atmospheric pressure outside the chamber from pushing the plunger in. Pushing the plunger in past the tolerance of the spring would shatter and ruin the detector.

2.2 Constructing the Chamber

Conducting this experiment in a vacuum chamber is essential to ensure purity of the deuterium gas. The chamber can be seen in Fig. 2.6. Both a micro-pirani gauge and an ion gauge on the vacuum system gave a vacuum pressure reading range of above atmosphere to below 0.1 μTorr. A

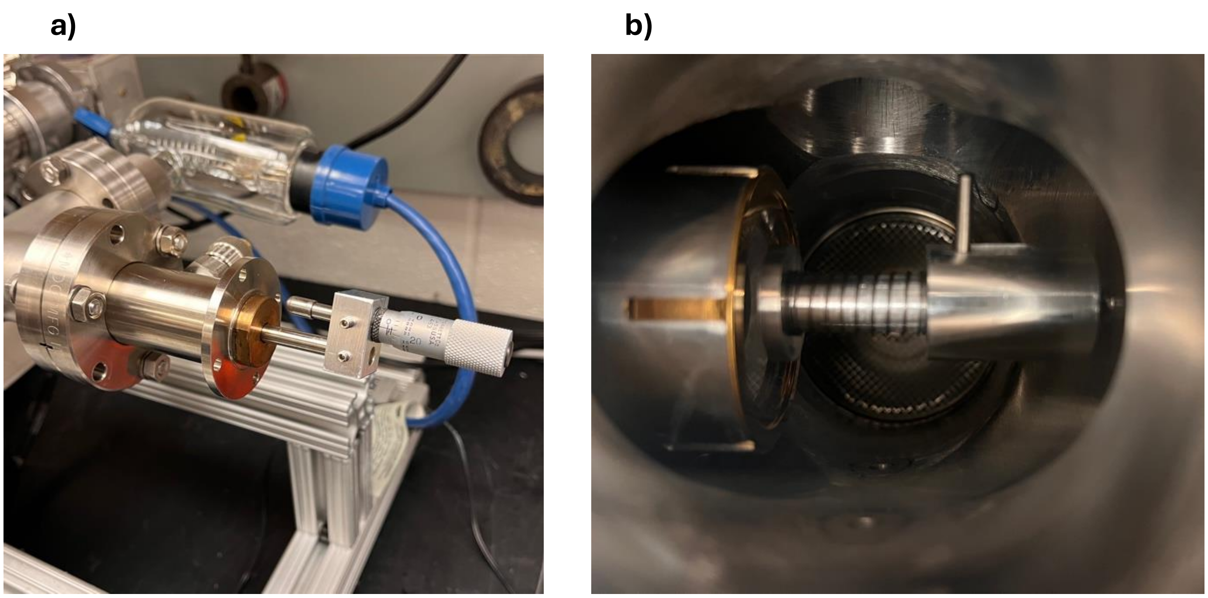

Figure 2.5 a) Vernier micrometer head on the plunger arm for precise control of the wafer's position. b) The spring, when pushed in, is right up against but not touching the detector.

turbomolecular pump and roughing pump in series evacuate the chamber of air. The RF plasma is optimized at a pressure of 400 mTorr and a power output of 12 watts. Valves attached to the turbo and the roughing pump allow the turbo to run cyclically when the plasma is on. This is important for conserving the deuterium gas during data collection, because deuterium is expensive.

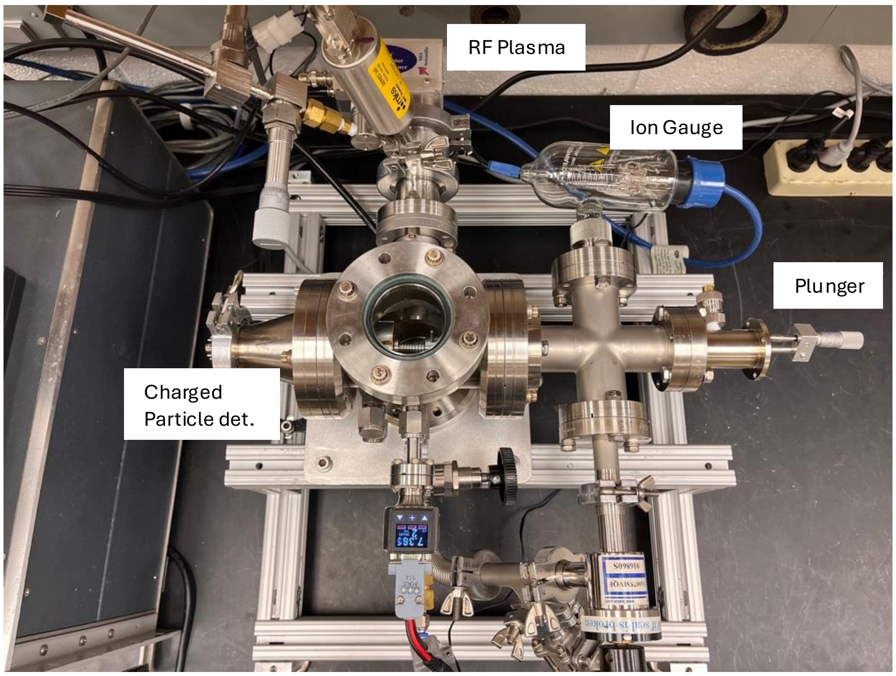

Figure 2.6 Full vacuum chamber used for the experiment. The RF plasma generator, ion gauge, plunger, and charged particle detector are labeled. The turbomolecular pump is beneath the system (into the page) and the roughing pump is below the bottom border of the picture.

2.3 Detectors

Two detectors are necessary for the experiment, the first of which is the charged-particle SBD. This is essential as not only does it record the charged particle fusion reaction products, but it also makes up half of the cavity. D-D fusion can take three paths:

$$d+d \rightarrow He^3+n \;\; ; \;\; d+d \rightarrow t+p \;\; ; \;\; d+d \rightarrow He^4+\gamma \tag{2.1}$$

with the first two having probability of about 50% each branch, and the last branch being extremely rare. The SBD is able to register the proton, triton, and helium 3 emissions and their energies. The SBD is a silicon diode that is thick enough to absorb the energies of these reaction products. The detector face has an aluminum coating thick enough to stop light. The detector is a p-type, reverse biased silicone diode. When a charged particle hits the detector, it will trigger an avalanche signal that is proportional to the energy of the particle. Reverse biasing the detector increases the depletion region in the silicon and gives higher energy resolution.

Neutrons do not register on the SBD as they are not charged. A separate detector is necessary to see neutrons. The neutron detector is made of neutron-capturing lithium-gadolinium-borate (LGB) crystals in a polyvinyl-toluene (PVT) matrix. Fig. 2.7 shows a picture of the LGB-PVT matrix. The neutrons enter the plastic PVT and collide with the hydrogen in the plastic. A proton is ejected from the polymer, taking the neutron's energy by momentum transfer. The proton deposits its energy through collisions in the scintillator, converting the energy into optical photons. This process of the neutron losing energy is called neutron thermalization. The LGB crystals have a larger cross section for thermal neutrons, and the LGB also scintillates from the capture reaction, creating a distinct shaped pulse. A photomultiplier tube (PMT) at the back of the detector collects the photons and outputs a characteristic 2-stage pulse from the proton recoil and neutron capture that can be analyzed. This pulse waveform is shown in Fig. 2.8. Through pulse-shape discrimination and time-of-flight, the energy of the neutron can be recovered.

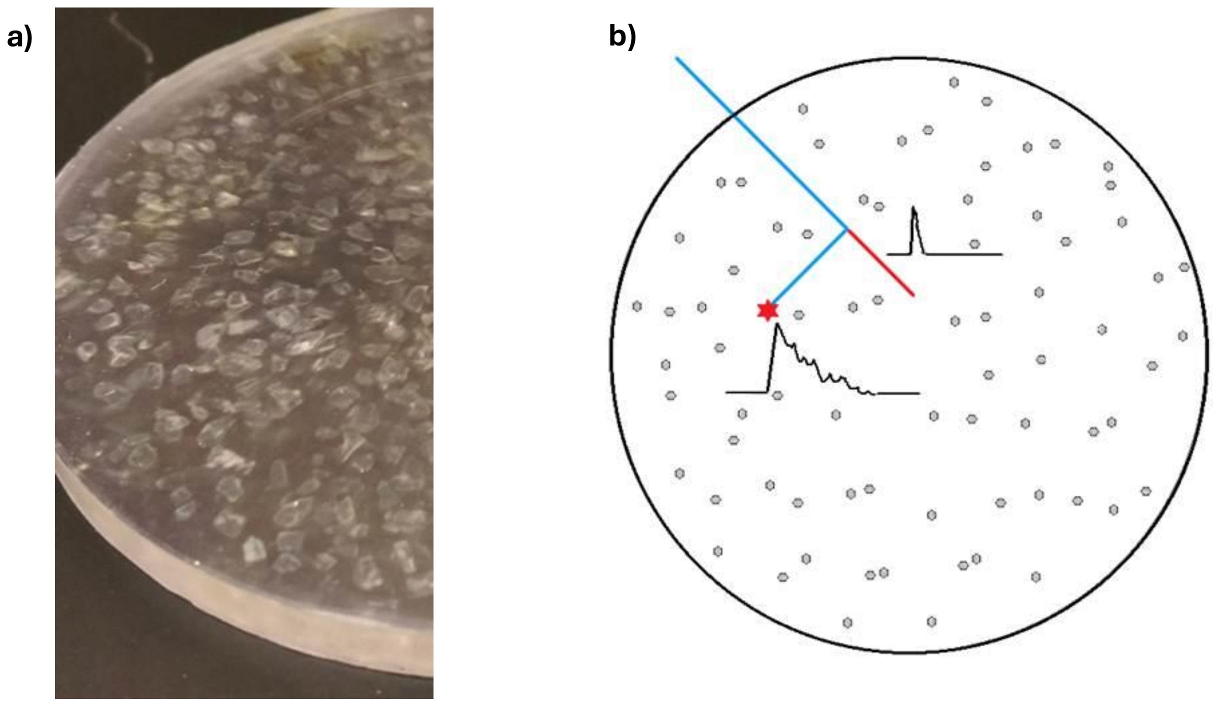

Figure 2.7 a) Lithium-gadolinium-borate (LGB) crystals in polyvinyl-toluene (PVT) plastic [14]. Both LGB and PVT are scintillating materials used in capture-gated neutron detectors. b) Diagram of neutron capture detection. The neutron enters the scintillating plastic from the outside, with the neutron's path shown in blue. The neutron hits a proton in the PVT plastic and transfers some its momentum to the proton, shown in red. The PVT plastic scintillates from moving proton and a sharp peaked pulse registers on the detector, shown adjacent to the red path. The neutron loses energy from momentum transfer and continues to move in the matrix until it is captured by the LGB crystal, shown by the star on the diagram. This capture causes another scintillating pulse, which is much more broad than the proton recoil pulse. Diagram was made by John Ellsworth, 2025.

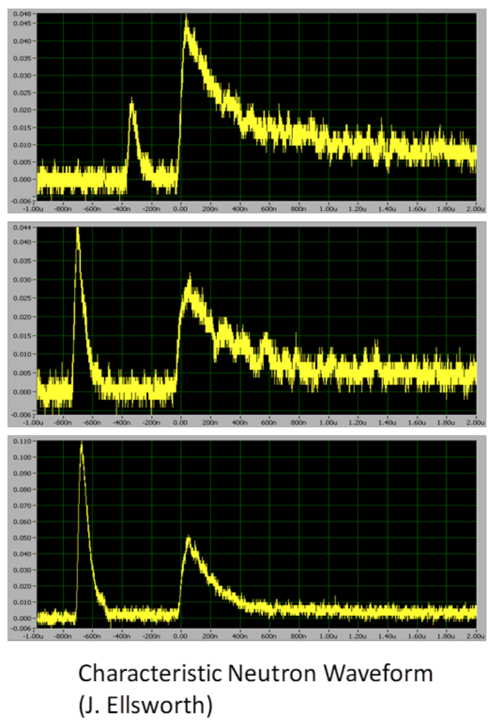

Figure 2.8 Typical waveforms of neutron capture. The figure shows 3 waveforms, each starting with a sharp proton recoil pulse followed by a broader neutron capture pulse. The neutron enters the detector matrix, and hits a proton in the polyvinyl-toluene (PVT) scintillator, causing the first scintillating peak. This is converted into a voltage signal by the photomultiplier tube (PMT) on the back of the PVT. The neutron continues to move in the plastic until it is captured by lithium-gadolinium-borate (LGB) crystals. This capture also leads to a broader scintillating pulse registered on the PMT. Waveform plot from John Ellsworth, 2004.

Chapter 3

Results

The vacuum chamber, after being built, had to be tested for leaks. I used a helium leak detector. This detector has its own roughing pump and turbo, coupled with a mass spectrometer calibrated for a mass of 4 amu. This is important to note because not only helium will be read. Leak checking was done before any deuterium entered the system. Molecular deuterium, having a mass of 4 amu, also registers on the detector as helium. After extensive checking, all of the leaks were sealed.

Another thing to consider is the Casimir force between the detector and the wafer. Theoretical estimates from the lab put the separation distance at 2.2 angstroms to get a shielding effect similar to a muonic atom, with anything closer than 40 nanometers necessary to get any effect at all [15]. I calculated the force at 2.2 angstroms to be over 40000 pounds, but at 2.2 nanometers it would only be 4 pounds. However, the model for Casimir forces assumes perfectly conducting plates, which silicon is not. For this reason, the estimates are an upper bound on the force required to separate the wafer and the SBD. I also looked at how the force would vary if the deposition was non-uniform. If one of the posts was centered over the top of the source, the other posts would be slightly shorter. Integrating over the area of the wafer, I found that the force would only vary within 1% regardless of post height if this were the case. Therefore, any effects of slightly unequal post heights from uneven deposition can be neglected. The calculations for this can be found in Appendix A.

The plasma generator is sensitive to pressure, requiring that the pressure be balanced at 400 mTorr and the power output be 12 watts. To balance the pressure, a vacuum line was connected from the turbo exhaust to the chamber with a bellows valve in series so that the turbo could run cyclically. After experimentation with air, the pressure was balanced at 400 mTorr which is optimal for the plasma generator.

The SBD was calibrated using an americium-241 source. Americium-241 has a well known spectrum for alpha decay. The detector can pick up these alphas and give a voltage response from the diode. An Ortec 428 detector bias supply biased the detector to -20 volts, increasing the depletion region in the diode and clearing up electrical noise. An Ortec 572 timing filter amplifier inverted and amplified the pulse shape. A CAEN digitizer binned the energy output. These digitized data points were analyzed with code, giving a spectrum output. The output for the americium source can be seen in Fig. 3.2. However, there is an issue with the calibration. As can be seen in the figure, the background peak on the left falls off with lower energy. This does not make sense. There should be one of two things expected, the first of which is that the background noise increases with decreasing energy. The other thing would be a sharp cutoff at a specific energy determined by the cutoff in the code. This is neither of those two, implying that there is an issue with the code or with the SBD itself.

I used Geant4 to try and model the neutron detector. Geant4 is a toolkit used to simulate particles passing through matter using Monte Carlo methods. I modeled an isotropic cone of neutrons with 2.45 MeV incident on LGB in PVT plastic. The code for the text geometry and macro files can be found in Appendices B and C respectively. I ran into issues getting the code to generate optical neutrons from scintillation that would be registered by the photomultiplier tube. The code accurately showed proton recoil events, as well as gamma rays produced from the neutron capture. Fig. 3.3 shows the wrl file generated from the code.

a) b)

Figure 3.1 a) HP 6213A power supply. This supply set the Vss -9 Volts to ground. b) Ortec detector electronics. The Ortec 428 power supply held the detector at -20 Volts to ground. The Ortec 572 timing filter amplifier inverted and amplified the pulse from the detector.

For the PVD chamber, the pressure gets down to 7 µTorr. This is important because of the mean free path of a particle at this pressure. I performed extensive leak testing on the PVD chamber as well to seal all leaks and ensure the pressure could get this low. The transformer on the system is rated for an output of 100 amps and 15 volts. That gives a max power of 1500 watts. A high current ammeter monitored the current drawn by the transformer. The current output was limited to 70 amps due to the tolerance of the tungsten filament. This was sufficient to heat up the substrate for thermal deposition. I also kept the variable auto transformer below 50% of the 120 volt maximum, which kept the power well within the desired range. Watching the tungsten filament for color change as the voltage slowly increased ensured the circuit operated properly. A picture of a deposition run can be seen in Fig. 3.4

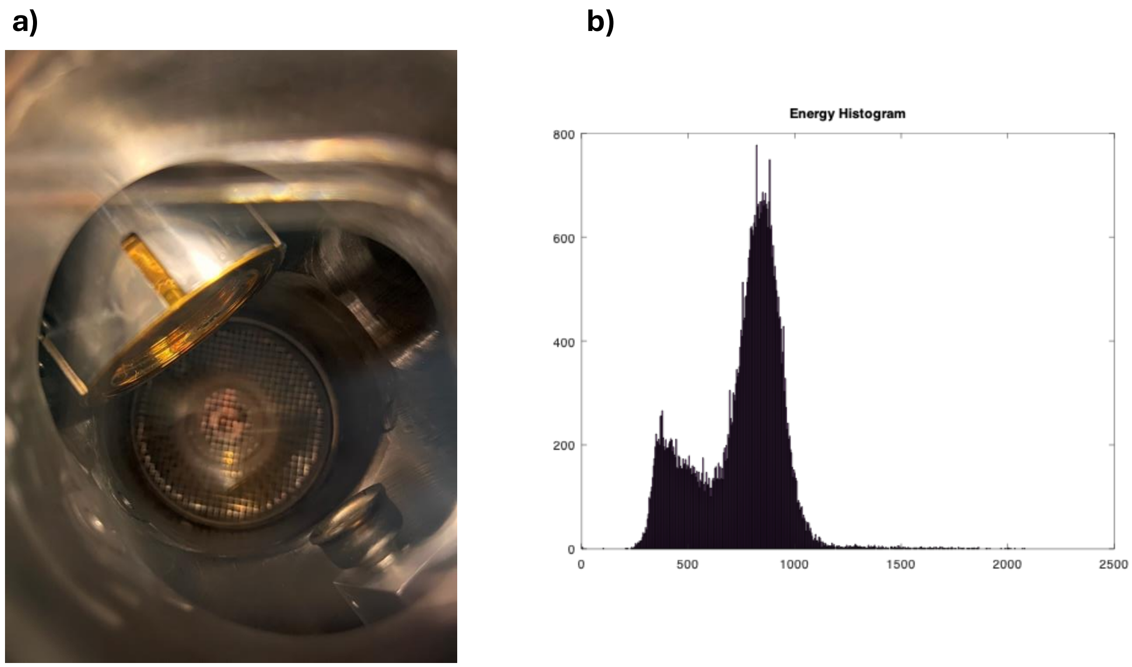

Figure 3.2 a) Americium-241 source (bottom left corner) incident on the charged particle detector. b) Histogram of the alpha particle energies. The x axis is in channels, which though this calibration process can be translated into energy. The right peak corresponds to 5.46 MeV, which is the value for americium-241. The left peak is background noise to be eliminated.

I wanted to deposit 20 angstroms of aluminum on the wafer to calibrate the QCM thickness gauge properly. After stopping deposition at 20 angstroms on the gauge, the target was taken to the ellipsometer to measure the thickness using the CompleteEase software. Using a model of aluminum oxide on silicon, the data was unable to be matched exactly. Trying fits with Cauchy and Oscillators, it was inconclusive. None of the standard optical models for the oxide layer worked to adequately fit the ellipsometric data. Trying to model the oxide layer with Cauchy, Gaussians, b-splines, etc. all indicated that the layer was very thin, less than 2 nm.

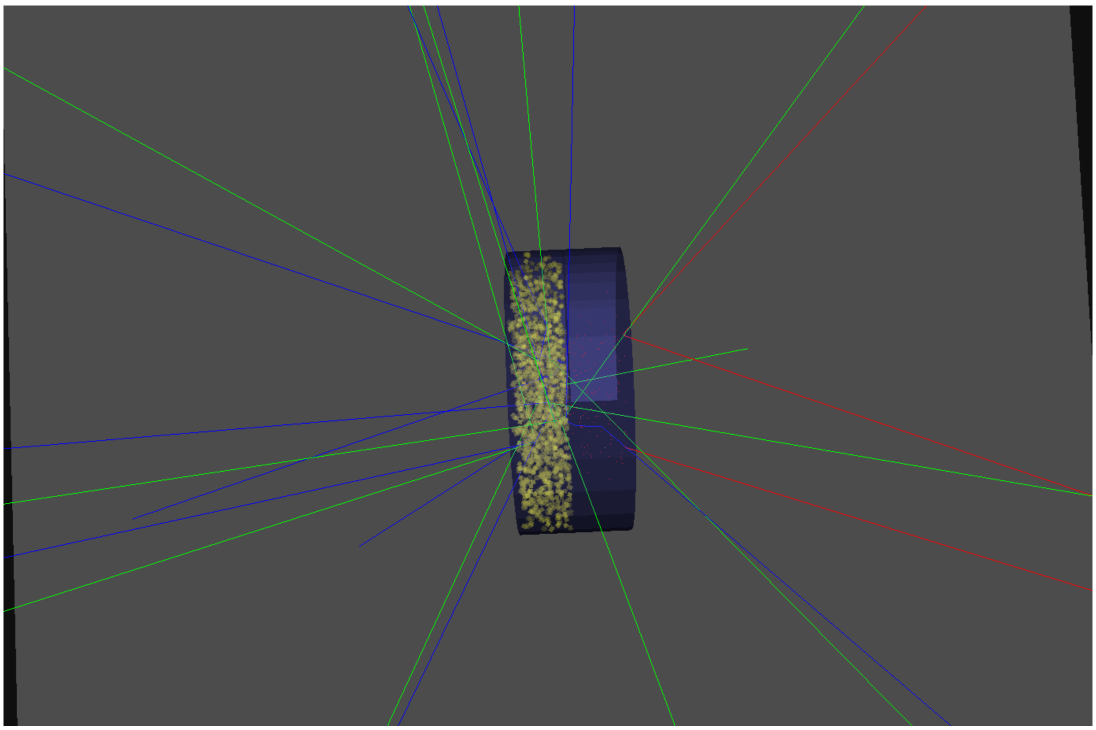

Figure 3.3 Geant4 neutron detector model. Isotropic neutrons at 2.45 MeV incident on polyvinyl-toluene (PVT) plastic with lithium-gadolinium-borate (LGB) crystals. The PVT is the blue cylinder and the LGB crystals are yellow cubes inside the blue cylinder. The incident particles were filtered out. Scattering and capture events can be seen with gammas in green, protons in red, and neutrons in blue. There are many proton recoil events in the PVT as expected, seen by the short red lines in the PVT. The gammas are from neutron capture events.

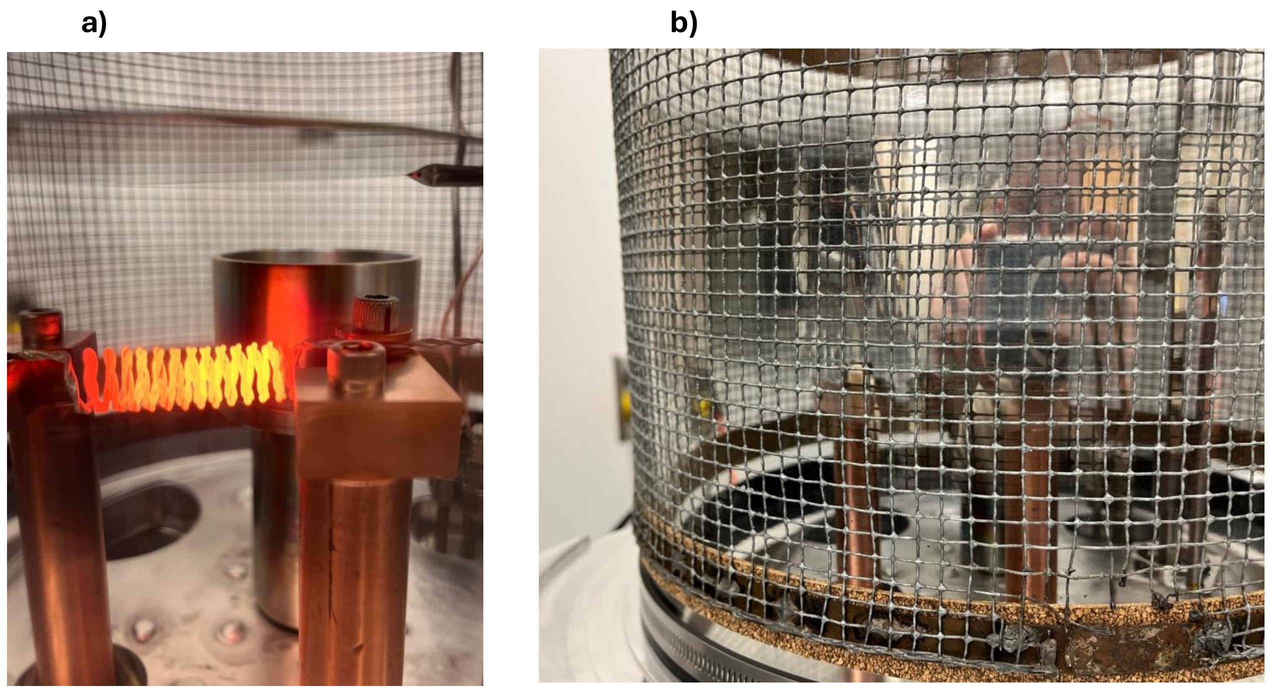

Figure 3.4 a) Tungsten filament being heated for deposition. b) Side of the chamber after a deposition run. Metal can be seen on the walls of the chamber from deposition.

Chapter 4

Conclusion

As stated earlier, Ellsworth proposed that intentionally made cavities on the surface of deuterated metals increased fusion rates of the deuterium [7]. The imperfections create cavities that influence the quantum vacuum field. Looking inside of the cavity made from parallel plates of a silicon wafer and a surface barrier detector allows for testing. The goal of this thesis is to show that the facility is adequate for making this measurement.

4.1 Analysis of the Results

The vacuum chamber holds vacuum well. The ultimate pressure is in the microtorr, which is sufficient to keep the deuterium gas clean. Helium leak detection showed that the system does not have a measurable leak. The pressure was successfully maintained at 400 mTorr, the pressure required by the plasma generator. At this pressure, the generator struck plasma, and the power output was the optimal 12 watts. This means that the chamber is adequate for the experiment.

The PVD chamber allowed for control over the spacing between the silicon wafer and the detector, which determined the size of the cavity. I put aluminum substrate into a tungsten filament and raised the current to 70 amps. This was enough heat to melt and evaporate the aluminum.

According to the theory work done by members of the lab, a thickness of less than 40 nanometers is required in order to see any change in fusion rates [15]. The INFICON STM-2 thin film monitor can resolve thicknesses to a tenth of an angstrom. This resolution is more than adequate. However, as mentioned above, the data could not be fit with ellipsometry models. The deposition left a visible layer of aluminum on the side of the chamber, meaning metallic aluminum evaporated quickly. There was most likely a mix of aluminum and aluminum oxide deposited on the target which affects the optical constants of the deposited material. After learning this, I moved the shutter from covering the substrate to covering the target in the chamber. This leaves the QCM open for constant deposition rate monitoring and hence finer control over target layer thickness. The next step is to deposit at least 10 nanometers onto several targets, which would give the ellipsometer more material to measure and yield a more accurate model for calibration.

The charged particle detector is not working. Results from the background run show a strange peak. This peak is not what is expected from electrical noise. The calibration trial using an americium source showed the same background peak alongside the alpha energy source peak. This meant that the alpha peak energy could not properly resolved. This lack of resolution meant the detector could not be calibrated. After moving all of the pulse shape analyzing equipment, the digitizer, and even the cables to a separate system with the same type of charged particle detector, this second detector behaved as expected and could resolve the americium alpha energy peak. Because the second detector behaved as expected, the original detector on the system was the problem. A new detector has been ordered. Further work can be done to calibrate this detector when it arrives.

As the facility currently stands, it is not adequate for measuring the products of D-D fusion and the experiment would be unsuccessful. However, there is potential to address every issue, such as ordering a new SBD and more tungsten filaments. There is also a neutron detector on hand that needs calibration. These three things, after being implemented, would make the facility feasible to perform the experiment.

4.2 Discussion of Relevance

This theory behind this thesis is directly related to Jones and Ellsworth's work in 2003 [7]. Looking directly at the cavity will determine if the cavity caused increased reaction rates. It is a falsifiable theory. One of the issues with testing this is the difficulty of measuring anything below 10^{-22} s^{-1} due to background noise.

The next steps of this experiment would be to run the facility. The steps are putting deuterium into the system, ionizing it with a plasma generator, and pushing the silicon wafer up against the detector. After extended runs, observing neutrons and charged particles with the characteristic energy of D-D fusion would support that the cavity is affecting the fusion rate.

After showing that the cavity helps, further work is to look for evidence that the reaction was electron-catalyzed. The evidence would be electrons that are emitted with energies of the fusion reaction. A high energy electron detector on the system would see the electrons. Further exploration can be done in the area of target fabrication, deuterization procedures, and low energy particle accelerators.

Instead of pushing two plates together, cavities can also be made entirely using PVD techniques. This is the reason why the PVD chamber is equipped with both thermal evaporation and sputtering sources. Using the two sources sequentially can create multilayer targets. Using titanium foil as a target, first evaporating an insulating dielectric onto the bulk titanium target and then sputtering more titanium onto the dielectric would create parallel layers of titanium. This can be deuterated in the same way as in reference [7], and placed in a chamber to measure any fusion products.

Lepton-catalyzed fusion is an important theory for nuclear fusion. The proof of electron catalyzed fusion would showcase a second lepton, after the muon, that is able to catalyze a fusion reaction. It implies that most fusion efforts are missing a step in their process to achieve sustained reactions. The implications go all the way to theories on the Sun's operation, requiring an adjustment in theories of plasma screening potentials.

Appendix A

Casimir Force Calculations

Casimir force calculations

Assume the aluminum evaporates isotropically., and is centered at the origin. Therefore, the thickness falls off as 1/r^2 because of the surface area of a sphere.

The shadow mask is in an equilateral triangle, 20mm apart. I will assume one of the posts is along the x axis. The target is 310mm above the substrate. The other two posts will have an equal radial distance from the substrate.

```
(*radial position of post on z axis*)
r = 310 * 10 ^ -3; (*m*)
(*distance between posts*)
d = 20 * 10 ^ -3; (*m*)
(*radial position of the other two posts*)
rp = √(d ^ 2 + r ^ 2);

(*thickness of the post along z*)
thick = 1 * 10 ^ -9; (*m*)
(*thickness of the other two posts*)
thick2 = thick * (r ^ 2)/(rp ^ 2);
```

In[149]:=

```
(*finding the relation of the height in z to the position y*)
(*The posts are equilateral, so the distance from a vertex to the base is 10 √3 *)
d1 = √(d ^ 2 - (d / 2) ^ 2);
(*slope is rise over run*)
m = (thick - thick2)/(d1);
b = (thick - m * d1 / 2);
z = m * y + b;
```

Now I will assume my target is actually a 1in by 1in square. This should overestimate the force.

```
(*the casimir force*)
```

In[153]:=

```
ℏ = 1.05457 * 10 ^ -34;
c = 2.9979 * 10 ^ 8 ;
F = N[Integrate[0.0254 * π^2 ℏ c/(240 z^4), {y, -0.0254 / 2, 0.0254 / 2}]]
P = F / 0.0254 ^ 2 * 0.000145038
```

Out[155]=

845 797.

Out[156]=

190 143.

In[157]:=

$$ni = \frac{\pi^2 \hbar c}{240\,(thick)^4}\ 0.000145038$$

Out[157]=

188 566.

In[158]:=

```
(P - ni) / ni
```

Out[158]=

0.00836447

Conclusion: The variation is within 1%.

In[139]:=

```
Clear["`*"]
```

Now to estimate the scale of the force.

In[161]:=

$$Fcasimir[l\_, a\_] = \frac{\pi^2 \hbar c}{240\,(l)^4}\ a$$

$$Pcasimir[l\_] = \frac{\pi^2 \hbar c}{240\,(l)^4}\ 0.000145038$$

Out[161]=

$$\frac{1.30011 \times 10^{-27}\ a}{l^4}$$

Out[162]=

$$\frac{1.88566 \times 10^{-31}}{l^4}$$

In[188]:=

```
Fcasimir[2.2 * 10 ^ -10, π * (0.0254 / 2) ^ 2]
Pcasimir[2.2 * 10 ^ -10] π * (0.0254 / 2) ^ 2
Fcasimir[2.2 * 10 ^ -9, π * (0.0254 / 2) ^ 2]
Pcasimir[2.2 * 10 ^ -9] π * (0.0254 / 2) ^ 2
```

Out[188]=

2.81221×10^{8}

Out[189]=

40 787.7

Out[190]=

28 122.1

Out[191]=

4.07877

At a separation of 2.2 angstroms, a one inch perfectly conducting wafer would take 40700 pounds to remove. On the other hand, increasing the separation to 2.2 nanometers lowers the force to 4 pounds.

Appendix B

Geant4 Neutron Detector Model Text Geometry File

```
// g4geom_tube.txt
// Geometry for a polyvinyl-toluene cyl with LGB:Ce crystal cubes


//------------------------------
// Parameters
//------------------------------
// Scintillator Dimensions
:P inch        25.4*mm
:P cylThick   0.4*$inch            // 10.16 mm
:P cylRadius  1.*$inch
:P cylHalfZ   5.*mm
// LGB Dimensions
:P lgbSide     0.75*mm
:P lgbHalf     0.5*$lgbSide


//------------------------------
// Basic rotations
//------------------------------
:ROTM R0 0. 0. 0.                    // identity rotation for cyl & world


//------------------------------
// World volume
//------------------------------
// Big enough box around the cyl
:VOLU world BOX 200.*mm 200.*mm 200.*mm G4_Galactic


//------------------------------
// Solid cylinder in PVT
//------------------------------
// TUBE: innerR outerR halfZ
// innerR = 0 → solid cylinder
:VOLU cyl TUBE  0. $cylRadius $cylHalfZ G4_PLASTIC_SC_VINYLTOLUENE
:VOLU ecyl TUBE 0. $cylRadius $cylHalfZ G4_PLASTIC_SC_VINYLTOLUENE

// Place cyl at origin inside world
:PLACE cyl 1 world R0 0. 0. 0.
:PLACE ecyl 2 world R0 0. 0. 1.*cm


//-----------------------------
// Make the Detector
//-----------------------------
// BOX: xHalf yHalf zHalf
//:VOLU det(S) BOX .375*cm .375*cm 100*micrometer G4_Si

// Place detector at the end of the tubes
//:PLACE det(S) 3 world R0 0. 0. 1.51*cm


// define the Li6 and B10 Isotope
:ELEM Li6 Li 3  3
:ELEM B10 B  5  5

// 4.2 is the density (g/ml). 4 is the number of components
// Follow each component by the number of atoms per unit (ratio)
// 10% LGB by weight or 3% by volume Steven-Howell-Senior-Thesis 2009
:MIXT_BY_NATOMS LGB_CE 4.2 4
  Li6 6 // make sure code is Lithium 6
  Gd  1 // make sure code Gadolinium 157
  B10 3  // make sure code is Boron 10
  O   9
  // Ce  0.001


//------------------------------
```

```
// LGB:Ce crystal cube logical volume
// TODO: define LGB_CE crystal
//----------------------------
// BOX: xHalf yHalf zHalf
// Material LGB_Ce must be defined elsewhere (C++ or another text file)
:VOLU lgbCube BOX $lgbHalf $lgbHalf $lgbHalf LGB_CE


//----------------------------
// Other optional Settings
//----------------------------
// Optional visibility settings
:VIS world   OFF
:VIS cyl    ON
:VIS lgbCube ON

// Optional colours (RGB in 0-1, alpha optional)
:COLOUR cyl    0.4 0.4 0.8 0.3     // gray, semi-transparent
:COLOUR lgbCube 0.8 0.8 0.1 0.0    // yellow
:COLOUR ecyl    0.4 0.4 0.8 0.3    // gray, semi-transparent
//:COLOUR det(S)  0.1 0.8 0.8 0.3    // cyan, semi-transparent

// Optional overlap checking
:CHECK_OVERLAPS * OFF


//----------------------------
// Include auto-generated random crystal placements
//----------------------------
#include lgb_crystals.txt

//Scintillation for PVT
//:prop G4_PLASTIC_SC_VINYLTOLUENE
//  SCINTILLATIONYIELD 10000./MeV
//  RESOLUTIONSCALE   1.0
//  SCINTILLATIONTIMECONSTANT1  2.4*ns
//  SCINTILLATIONYIELD        1.0
//  photon_energies 3  2.7*eV 3.0*eV 3.3*eV
//  RINDEX    1.58 1.58 1.58
//  ABSLENGTH 3.*m 3.*m 3.*m
#include PVTInterp.tg

:prop G4_Galactic
  photon_energies 2 2.5*eV 5.0*eV
  RINDEX 1 1

//Scintillation for LGB_CE
//:prop LGB_CE
  //SCINTILLATIONYIELD 20000./MeV
  //RESOLUTIONSCALE   1.0
  //SCINTILLATIONTIMECONSTANT1  40.*ns
  //photon_energies 3  2.75*eV 2.95*eV 3.10*eV
  //RINDEX    1.80 1.80 1.80
  //ABSLENGTH 80*cm 80*cm 80*cm
  //SCINTILLATIONCOMPONENT1 1.0 1.0 1.0

//:surf <name> <vol1>:<copyNo1> <vol2>:<copyNo2>
//:surf LGBskin lgbCube
  //type dielectric_dielectric
  //model unified
  //finish ground
  //sigma_alpha 0.1
  //property photon_energies 3 2.5*eV 3.0*eV 4.0*eV
    //REFLECTIVITY 0.9 0.9 0.9

// end scintillation
```

Appendix C

Geant4 Neutron Detector Model Macro File

```
#https://www.fe.infn.it/u/paterno/Geant4_tutorial/slides_further/GPS/GPS_manual.pdf


##using wrl
/geometry/source neutronDetector.tg

# add physics lists DOES NOT WORK? Test on West wall computer, not Lnar2
/physics_lists/select QGSP_BERT_HP_EMV
#cmd below is availabe only after the cmd above is used
/physics_lists/factory/addOptical
#/physics_lists/factory/addNeutronHP

/run/initialize

/process/optical/verbose 1
/vis/ASCIITree/verbose 13
/vis/drawTree
/geometry/test/run

##G4 General Particle Source (gps)
/gps/particle neutron
/gps/energy 2.45 MeV

/gps/pos/centre 0 0 -4 cm    # Set the source position at the origin (or near it)

# Set the initial direction along the positive x-axis
/gps/direction 0 0 1

# Define angular distribution for hemispherical emission
/gps/ang/type iso  # Iso is documented as the default, but it is not
#/gps/ang/type cos
/gps/ang/mintheta 165 deg      # Min polar angle
/gps/ang/maxtheta 180 deg     # Max polar angle (90 degrees for hemisphere)
/gps/ang/minphi 0 deg        # Azimuthal angle range (0 degrees)
/gps/ang/maxphi 360 deg      # Full azimuthal angle (360 degrees to cover all around)

# Set colors to particles
/vis/modeling/trajectories/create/drawByParticleID
/vis/modeling/trajectories/drawByParticleID-0/set gamma green
/vis/modeling/trajectories/drawByParticleID-0/set neutron blue
/vis/modeling/trajectories/drawByParticleID-0/set proton red
/vis/modeling/trajectories/drawByParticleID-0/set e- black

/vis/scene/endOfEventAction accumulate


# Filters out all primary trajectories, leaving only the products
/vis/filtering/trajectories/create/attributeFilter secondaries
/vis/filtering/trajectories/secondaries/setAttribute PID
/vis/filtering/trajectories/secondaries/addValue 0
/vis/filtering/trajectories/secondaries/invert true

/run/beamOn 5000


# For the WRL viewer
/vis/open VRML2FILE
/vis/viewer/zoom 1
/vis/viewer/set/background white ! ! 0
/vis/drawVolume

# Save to a root file
# Open and edit by putting 'root filename.root' in the terminal
# See https://root-forum.cern.ch/t/view-contents-of-root-file-like-a-csv-viewer/51604 for more information
/analysis/setFileName data1.root


/vis/scene/add/trajectories
```

```
/vis/scene/endOfEventAction accumulate

# fix the result
/random/setSeeds 23 234 53 89 157
/run/beamOn 5000
```

Bibliography

[1] K. S. Krane, *Introductory Nuclear Physics* (Wiley, New York, 1987), p. 535.

[2] E. E. Salpeter, “Electrons Screening and Thermonuclear Reactions,” Australian Journal of Physics **7,** 373 (1954).

[3] F. C. Frank, “Hypothetical Alternative Energy Sources for the ’Second Meson’ Events,” Nature **160,** 525–527 (1947).

[4] A. D. Sakharov, “Passive Mesons (Translated into English),” Muon Catalyzed Fusion **4,** 235–239 (1989).

[5] L. W. Alvarez *et al.*, “Catalysis of Nuclear Reactions by μ Mesons,” Phys. Rev. **105,** 1127–1128 (1957).

[6] S. E. Jones *et al.*, “Observation of unexpected density effects in muon-catalyzed d-t fusion,” Phys. Rev. Lett. **56,** 588–591 (1986).

[7] F. Keeney, S. Jones, A. Johnson, P. Hagelstein, D. Buehler, F. Cecil, M. Scott, and J. Ellsworth, “Charged-Particle Emissions from Deuterided Metals,” Condensed Matter Nuclear Science pp. 509–523 (2005).

[8] J. E. Ellsworth, Private communication (2025).

[9] M. Lipoglavšek, S. Markelj, M. Mihovilovič, T. Petrovič, S. Štajner, M. Vencelj, and J. Vesić, "Observation of electron emission in the nuclear reaction between protons and deuterons," Physics Letters B **773,** 553–556 (2017).

[10] S. Koonin and M. Nauenberg, "Koonin and Nauenberg 1989: spontaneous fusion in a deuterium molecule - a starting point for low temperature D+D fusion rate discussions," Nature 339 (1989).

[11] P. Milloni, *The Quantum Vacuum: An Introduction to Quantum Electrodynamics*, 1st ed. (Academic Press, San Diego, CA, 1994).

[12] H. E. Puthoff, "Ground state of hydrogen as a zero-point-fluctuation-determined state," Physical review D: Particles and fields **35,** 3266–3269 (1987).

[13] S. Bulavenko, P. Melnik, M. Nakhodkin, and A. Goriachko, "Investigation of hydrogen interaction with the Si(111)-7×7 surface by STM with Bi/W tips," Surface Science **600,** 1185–1192 (2006).

[14] K. Terry, "Paired Neutron Detection," Senior thesis (Brigham Young University, Provo, U.T., 2016).

[15] T. Hamm, "Lepton-Catalyzed Nuclear Fusion: Quantum Cavity Modulated Fusion (To Be Published)," Senior thesis (Brigham Young University, Provo, U.T., 2026).

Index